INTERNATIONAL JOURNAL FOR NUMERICAL METHODS IN FLUIDS
Int. J. Numer. Meth. Fluids 2009; **59**:423–442
Published online 17 June 2008 in Wiley InterScience (www.interscience.wiley.com). DOI: 10.1002/fld.1823

An improvement of classical slope limiters for high-order discontinuous Galerkin method

R. Ghostine[1,*,†], G. Kesserwani[1], R. Mosé[1], J. Vazquez[1] and A. Ghenaim[2]

[1]*U.P.R. Systèmes Hydrauliques Urbains, Ecole Nationale du Génie de l'Eau et de l'Environnement de Strasbourg, 1 quai Koch BP 61039 F, 67070 Strasbourg Cedex, France*
[2]*INSA, Institut National des Sciences Appliquées, 24 boulevard de la Victoire, 67084 Strasbourg Cedex, France*

SUMMARY

In this paper, we describe some existing slope limiters (Cockburn and Shu's slope limiter and Hoteit's slope limiter) for the two-dimensional Runge–Kutta discontinuous Galerkin (RKDG) method on arbitrary unstructured triangular grids. We describe the strategies for detecting discontinuities and for limiting spurious oscillations near such discontinuities, when solving hyperbolic systems of conservation laws by high-order discontinuous Galerkin methods. The disadvantage of these slope limiters is that they depend on a positive constant, which is, for specific hydraulic problems, difficult to estimate in order to eliminate oscillations near discontinuities without decreasing the high-order accuracy of the scheme in the smooth regions. We introduce the idea of a simple modification of Cockburn and Shu's slope limiter to avoid the use of this constant number. This modification consists in: slopes are limited so that the solution at the integration points is in the range spanned by the neighboring solution averages. Numerical results are presented for a nonlinear system: the shallow water equations. Four hydraulic problems of discontinuous solutions of two-dimensional shallow water are presented. The idealized dam break problem, the oblique hydraulic jump problem, flow in a channel with concave bed and the dam break problem in a converging–diverging channel are solved by using the different slope limiters. Numerical comparisons on unstructured meshes show a superior accuracy with the modified slope limiter. Moreover, it does not require the choice of any constant number for the limiter condition. Copyright © 2008 John Wiley & Sons, Ltd.

Received 23 November 2007; Revised 12 March 2008; Accepted 13 March 2008

KEY WORDS: discontinuous Galerkin method; two-dimensional shallow water equations; slope limiter; steady; transient; unstructured grids

1. INTRODUCTION

The success of the discontinuous Galerkin methods in approximating various physical problems, notably hyperbolic systems of conservative laws, has attracted the hydraulic engineering

*Correspondence to: R. Ghostine, U.P.R. Systèmes Hydrauliques Urbains, Ecole Nationale du Génie de l'Eau et de l'Environnement de Strasbourg, 1 quai Koch BP 61039 F, 67070 Strasbourg Cedex, France.
†E-mail: rabih.ghostine@engees.u-strasbg.fr

communities to explore the benefits of this approach [1–4]. One favorable property of the discontinuous Galerkin methods is that they conserve mass at the element level in a finite element framework. Consequently, they inherit the flexibility of finite elements in handling complicated geometries and require a simple treatment of boundary conditions and source terms to obtain high-order accuracy.

First-order schemes are the only approaches that maintain a monotonic solution structure at discontinuities. Moreover, numerical diffusion due to upwinding is big enough to keep the scheme stable [5–7]. Unfortunately, these schemes represent the solution with an excessive amount of dissipation. High-order numerical schemes produce spurious oscillations near discontinuities, which may lead to numerical instabilities and unbounded computational solutions. Even if the oscillations are less severe, they produce non-physical solutions, such as negative water depths, which is unacceptable. In such a case, the use of an appropriate slope limiter is crucial to ensure the stability of the method.

In one-dimensional space, discontinuous finite elements can be interpreted as a generalization of high-order Godunov finite differences [8–11]. Such high resolution schemes are usually stabilized using some form of TVD limiters [12, 13] so that spurious oscillations can be avoided without destroying the high-order accuracy of the schemes. One commonly used technique is the Van Leer's MUSCL slope limiter [11].

In multi-dimensional spaces, the Runge–Kutta discontinuous Galerkin (RKDG) method is still facing difficulties to attain the same degree of accuracy as in the one-dimensional case, especially on unstructured meshes. The troublesome part is the construction of appropriate multi-dimensional slope limiters that preserve the accuracy of the scheme. Consequently, a great deal of effort has been oriented for the construction of genuine multi-dimensional slope limiters that can eliminate unphysical oscillations without adding excessive numerical viscosity.

Cockburn and Shu [1, 2, 14, 15] extended the Van Leer's MUSCL slope limiter to the so-called generalized slope limiter where a $(k+1)$th-order of accuracy is achieved in smooth regions by using the DG method with polynomials of degree k for the spatial discretization and a special $(k+1)$th-order explicit Runge–Kutta method for temporal discretization. The generalized slope limiter does not totally smear oscillations near shocks, but it preserves the accuracy of the scheme in smooth regions. Thus, the resulting scheme is not TVD; however, it satisfies a TVB property.

Hoteit [16] and Hoteit *et al.* [17] concentrated on a genuinely multi-dimensional slope limiter in the sense that it does not require any operator splitting. This slope limiting operator was introduced by Chavent and Jaffré [18] as a generalization of Van Leer's MUSCL limiter [11]. The main idea of this new reconstructing and limiting technique follows a well-known approach where local maximum principle is defined by enforcing some constraints on the reconstruction of the solution, as the mass conservation.

In this work, we introduce a simple modification of Cockburn and Shu's slope limiter for the solution to the two-dimensional shallow water equations on arbitrary unstructured triangular grids. The main idea of this modification and limiting technique is to change the limiter condition to avoid the use of a constant positive number, which can be difficult to fix for specific hydraulic problems. Therefore, slopes are limited so that the solution at the integration points is in the range spanned by the neighboring solution averages. Numerical tests on the idealized dam break problem, the oblique hydraulic jump problem, flow in a channel with concave bed and the dam break problem in a converging–diverging channel show that the modified slope limiter can eliminate unphysical oscillations and that the high order of the scheme is preserved in the smooth regions.

DOI: 10.1002/fld

The outline of the remainder of the paper is as follows. In Sections 2 and 3, we describe the mathematical model and the numerical scheme, respectively. Section 4 presents some existing slope limiter and the modified slope limiter. Computational results on a variety of test cases are presented in Section 5 with conclusions following in Section 6.

2. MATHEMATICAL MODEL

The two-dimensional depth-integrated shallow water equations are obtained by integrating the Navier–Stokes equations over the flow depth with the following assumptions: uniform velocity distribution in the vertical direction, incompressible fluid, hydrostatic pressure distribution and small bottom slope. The continuity and momentum equations are

$$\frac{\partial U}{\partial t}+\frac{\partial E}{\partial x}+\frac{\partial G}{\partial y}=S \tag{1}$$

in which

$$U=\begin{pmatrix} h \\ hu \\ hv \end{pmatrix}, \quad E=\begin{pmatrix} hu \\ hu^2+gh^2/2 \\ huv \end{pmatrix}, \quad G=\begin{pmatrix} hv \\ huv \\ hv^2+gh^2/2 \end{pmatrix}$$

and

$$S=S_0+S_f=\begin{pmatrix} 0 \\ ghS_{0x} \\ ghS_{0y} \end{pmatrix}+\begin{pmatrix} 0 \\ -ghS_{fx} \\ -ghS_{fy} \end{pmatrix} \quad \text{is the source term}$$

where u and v are the velocity components in the x and y directions, respectively; h is the water depth; g is the acceleration due to gravity; (S_{0x}, S_{0y}) are the bed slopes in the x and y directions and (S_{fx}, S_{fy}) are the friction slopes in the x and y directions, respectively. In this study, the friction slopes are estimated by using Manning's formula:

$$S_{fx}=\frac{n_{\mathrm{M}}^2 u\sqrt{u^2+v^2}}{h^{4/3}}, \quad S_{fy}=\frac{n_{\mathrm{M}}^2 v\sqrt{u^2+v^2}}{h^{4/3}}$$

where n_{M} is Manning's roughness coefficient.

3. NUMERICAL APPROXIMATION

We consider a finite element discretization of the field of calculation $\Omega=\bigcup_{i=1}^{M} K_i$, where K_i is a triangular element. We describe the space and temporal approximations below, and the results of stability.

DOI: 10.1002/fld

3.1. Space discretization

Let $V = L^2(\Omega \times [0, \infty[)$ be the space of the solutions of Equation (1), and let the approximate space $V_h^k \subset V$ be defined by

$$V_h^k = \{v \in V / v/_{T_i} \in P^k,\ i = 1, \ldots, M\}$$

where P^K is the space of the polynomials of degree k ($k = 1, 2, \ldots$). Consequently, the solutions v are discontinuous from a triangle to another. Subsequently, we will fix $k = 1$. In order to build a solution $U_h \in V_h^1$, we multiply Equation (1) by a test function $v_h(x, y) \in V_h^1$, and we integrate on each triangle K. The obtained system is written for $U_h = U/_K$

$$\frac{\mathrm{d}}{\mathrm{d}t} \int_K U_h(x, y, t) v_h(x, y)\, \mathrm{d}K + \int_K \nabla F(U_h(x, y, t)) v_h(x, y)\, \mathrm{d}K = \int_K S(U_h(x, y, t)) v_h(x, y)\, \mathrm{d}K \tag{2}$$

where $F = (E, G)$ and after integration by parts, we obtain

$$\frac{\mathrm{d}}{\mathrm{d}t} \int_K U_h(x, y, t) v_h(x, y)\, \mathrm{d}K = \int_K F(U_h(x, y, t)).\nabla v_h(x, y)\, \mathrm{d}K - \int_{\partial K} F(U_h(x, y, t)).n_k v_h(x, y)\, \mathrm{d}\Gamma + \int_K S(U_h(x, y, t)) v_h(x, y)\, \mathrm{d}K \tag{3}$$

Here $n_k = (n_x, n_y)$ is the unit vector outward normal to the element boundary Γ of the finite element K.

The approximated variable U_h can be expressed as a sum of the products of discrete variables U_i and shape functions φ_i

$$U_h(x, y) = \sum_i U_i \varphi_i(x, y) \tag{4}$$

Using the standard Galerkin approach, shape functions and test functions are identical. Rewriting Equation (3), the discontinuous Galerkin space discretization can be summarized by a system of ordinary differential equations as

$$\frac{\mathrm{d}}{\mathrm{d}t} M U_h = L_{h,U}(U_h) \tag{5}$$

where M is the mass matrix and L_h is an operator describing the spatial discretization.

By using orthogonal shape functions, the mass matrix M in the linear equation system (5) becomes diagonal. For triangular elements, a linear shape function can be obtained by choosing a function that takes the value of 1 at the midpoint m_i of the ith edge of a triangle and the value of 0 at the midpoints of the other two edges. Thus, the diagonal mass matrix can be expressed as follows:

$$M = |K| \operatorname{diag}(\tfrac{1}{3}, \tfrac{1}{3}, \tfrac{1}{3}) \tag{6}$$

DOI: 10.1002/fld

The integrals are approximated by a three-midpoint rule for the triangles and a two-point Gauss integration for the line integrals [19].

3.2. Numerical flux

The approximation of the numerical flux for the discontinuous Galerkin method is identical to the approximated solution to a Riemann problem according to finite-volume methods. By using linear or higher subcell resolution for higher-order discontinuous Galerkin methods, the scheme gets less sensitivity to the choice of the numerical flux than the Godunov-type methods. In that case, a simple Lax–Friedrich flux gives good results:

$$F(U_{\mathrm{L}}, U_{\mathrm{R}})\cdot n = \tfrac{1}{2}[(F(U_{\mathrm{L}}) + F(U_{\mathrm{R}}))\cdot n - a_{\max}(U_{\mathrm{R}} - U_{\mathrm{L}})] \tag{7}$$

where $a_{\max} = \max(|a^1|, |a^2|, |a^3|)$, and a^k $(k = 1, \ldots, 3)$ are the eigenvalues of the Jacobian matrix:

$$\widetilde{A} = \frac{\partial(F\cdot n)}{\partial U} = \begin{bmatrix} 0 & n_x & n_y \\ (c^2 - u^2)n_x - uvn_y & 2un_x + vn_y & un_y \\ (c^2 - u^2)n_y - uvn_x & vn_x & un_x + 2vn_y \end{bmatrix}$$

and $c = \sqrt{gh}$ is the wave celerity.

3.3. Time integration

The second-order accurate, two-stage TVD Runge–Kutta schemes of Cockburn and Shu [2] are employed in this work. An optimal second-order TVD Runge–Kutta method is given by

$$\begin{aligned} U_h^1 &= U_h^n + \mathrm{d}t\cdot L_{h,U}(U_h^n) \\ U_h^{n+1} &= \tfrac{1}{2}(U_h^n + U_h^1 + \mathrm{d}t\cdot L_{h,U}(U_h^1)) \end{aligned} \tag{8}$$

Since the TVD Runge–Kutta method is an explicit scheme, the time step $\mathrm{d}t$ must be selected based on the Courant–Friedrich–Lewy stability criterion. The maximum allowable time step is limited in this paper by the following criteria:

$$\mathrm{d}t = \mathrm{CFL}\frac{|K|}{\sum_{j=1}^{3} l_j \min(u\cdot n_x + v\cdot n_y - c, 0)} \tag{9}$$

where l_j is the length of the edge of the cell K and $0 < \mathrm{CFL} \leqslant 1$ is the Courant number.

4. EXISTING SLOPE LIMITERS

In this section, we briefly review two slope limiters introduced by Cockburn and Shu [2] and by Hoteit [16] and Hoteit *et al.* [17] for triangular grids. We restrict the presentation for P^1 piecewise approximation functions on triangular elements. The degrees of freedom are the state values at the midpoints of the grid edges.

DOI: 10.1002/fld

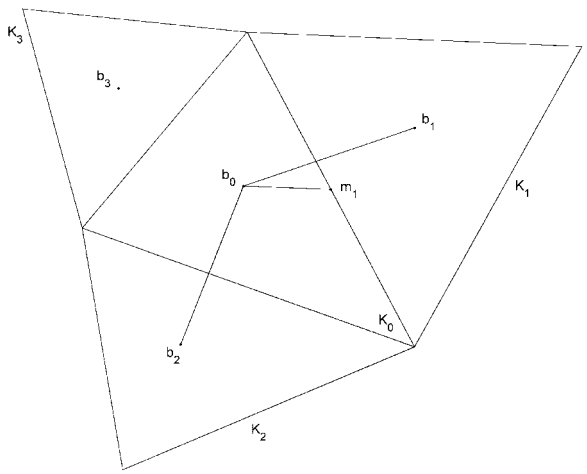

Figure 1. Slope limiting for triangular elements.

4.1. Slope limiter of Cockburn and Shu

To describe the limiter, we use the same notations as in Cockburn and Shu [2]. For an arbitrary triangle K_0 and its surrounding neighbors K_i, $i=1,\ldots,3$, the notations b_i, $i=0,\ldots,3$, and m_i, $i=1,\ldots,3$, refer, respectively, to the barycenters of the triangles and the midpoints of the edges within K_0 (Figure 1).

Choosing any edge midpoint m_1, we obtain

$$m_1-b_0=\alpha_1(b_1-b_0)+\alpha_2(b_2-b_0) \quad \text{for some } \alpha_1,\alpha_2\in\mathbb{R}^{+2} \tag{10}$$

For any linear function u_h, the mean gradient can be expressed as

$$\Delta\overline{u}(m_1,K_0)=\alpha_1(u_h(b_1)-u_h(b_0))+\alpha_2(u_h(b_2)-u_h(b_0)) \tag{11}$$

By using the basis functions φ_i, u_h can be expressed over K_0 as follows:

$$u_h(x,y)=\sum_{i=1}^{3}u_h(m_i)\varphi_i(x,y)=u_h(b_0)+\sum_{i=1}^{3}(u_h(m_i)-u_h(b_0))\varphi_i(x,y) \tag{12}$$

First, we compute the quantities:

$$\Delta_i=\widetilde{m}(u_h(m_i)-u_h(b_0),\nu\Delta\overline{u}(m_i,K_0)) \quad \text{for some } \nu>1 \tag{13}$$

where ν is a positive constant number equal to 1.5 and $\widetilde{m}$ is the TVB minmod function defined as follows:

$$\widetilde{m}(a_1,a_2)=\begin{cases}a_1 & \text{if } |a_1|\leqslant M(\Delta x)^2\\ m(a_1,a_2) & \text{otherwise}\end{cases} \tag{14}$$

DOI: 10.1002/fld

where M is a given positive constant; and m is the minmod function, defined as follows:

$$m(a_1, a_2) = \begin{cases} s \min\limits_{1 \leqslant n \leqslant 2} |a_n| & \text{if } s = \text{sign}(a_1) = \text{sign}(a_2) \\ 0 & \text{otherwise} \end{cases} \tag{15}$$

Consequently, reconstruction is carried out according to the following two cases:

1. If $\sum_{i=1}^{3} \Delta_i = 0$, the new midpoint value is given by

$$u_h(m_i) = u_h(b_0) + \sum_{i=1}^{3} \Delta_i \varphi_i(x, y) \tag{16}$$

2. If $\sum_{i=1}^{3} \Delta_i \neq 0$, we compute

$$\text{pos} = \sum_{i=1}^{3} \max(0, \Delta_i), \quad \text{neg} = \sum_{i=1}^{3} \max(0, -\Delta_i) \tag{17}$$

and define

$$\theta^+ = \min\left(1, \frac{\text{neg}}{\text{pos}}\right), \quad \theta^- = \min\left(1, \frac{\text{pos}}{\text{neg}}\right) \tag{18}$$

Finally, the new midpoint value is given by

$$u_h(m_i) = u_h(b_0) + \sum_{i=1}^{3} \widehat{\Delta}_i \varphi_i(x, y) \tag{19}$$

where

$$\widehat{\Delta}_i = \theta^+ \max(0, \Delta_i) - \theta^- \max(0, -\Delta_i) \tag{20}$$

Since the shallow water equations are a system of equations, the limiting must be performed in the local characteristic variables in the direction of vector $m_1 - b_0$. The variables are therefore transformed by T^{-1} into the characteristic space, where T is the matrix of right eigenvectors of the following Jacobian:

$$\partial_U (E(U(b_0)), G(U(b_0))) \cdot \frac{m_i - b_0}{|m_i - b_0|} \tag{21}$$

4.2. Modified slope limiter of Cockburn and Shu

We have seen that the TVB minmod function defined in Equation (14) depends on the constant positive number M. The choice of this number depends on the solution to the problem and the mesh of the domain. This can make it difficult to choose this number to eliminate unphysical oscillations and preserve the high-order accuracy of the scheme in the smooth regions. In our work, we introduce here a simple modification in the TVB minmod function to avoid the use of the constant number M. Slopes are limited so that the solution at the midpoints of the edges is in the range spanned by the neighboring solution averages:

$$\overline{U}_{K_0}^{\min} \leqslant u_h(m_i) \leqslant \overline{U}_{K_0}^{\max} \quad \text{for } i = 1, 2, 3 \tag{22}$$

where $\overline{U}_{K_0}^{\min}$, $\overline{U}_{K_0}^{\max}$ are the minimum and maximum element averaged solution on the elements sharing faces with the cell K_0, respectively.

DOI: 10.1002/fld

$\overline{U}_{K_0}^{\min} = \min(u_h(b_1), u_h(b_2), u_h(b_3))$ and $\overline{U}_{K_0}^{\max} = \max(u_h(b_1), u_h(b_2), u_h(b_3))$ and the quantity Δ_i defined in Equation (13) is expressed as follows:

$$\Delta_i = \begin{cases} u_h(m_i) - u_h(b_0) & \text{if } \overline{U}_{K_0}^{\min} \leqslant u_h(m_i) \leqslant \overline{U}_{K_0}^{\max} \\ m(u_h(m_i) - u_h(b_0), v\Delta\overline{u}(m_i, K_0)) & \text{otherwise} \end{cases} \tag{23}$$

Therefore, the modified slope limiter depends only on the solutions at the neighboring cells and does not require any choice of specific constant for the limitation, as it is the case in Cockburn and Shu [2].

4.3. Slope limiter of Hoteit et al.

To describe the slope limiting procedure, let us consider a triangular element K_0 surrounded by its neighborhoods K_i, $i = 1, \ldots, 3$ (Figure 1). The aim is to reconstruct the average values $\widetilde{u}_h(m_i)$ at the midpoints of the edges. An indispensable condition that must be satisfied is the local mass conservation. To obey a local maximum principle, some constraints are imposed to ensure that each reconstruction $u_h(m_i)$ is between the cell averages of the two adjacent elements. To have a less restrictive limiting, the reconstructions $u_h(m_i)$ are kept as close as possible to the initial state values $\widetilde{u}_h(m_i, K_0)$. The resulting optimization problem to solve is therefore as follows.

For given initial state values $(\widetilde{u}_h(m_1), \widetilde{u}_h(m_2), \widetilde{u}_h(m_3))$, find $u_h(b_0)$ the solution to the problem:

$\min_W \|W - \widetilde{u}_h(b_0)\|_2$, subject to the linear constraints:

$$W(b_0) = \tfrac{1}{3}(u_h(m_1) + u_h(m_2), u_h(m_3)) = u_h(b_0) \tag{24}$$

$$\begin{aligned} &(1-\alpha)\widetilde{u}_h(b_0) + \alpha\min(\widetilde{u}_h(b_1), \widetilde{u}_h(b_0)) \leqslant u_h(m_1) \leqslant (1-\alpha)\widetilde{u}_h(b_0) + \alpha\max(\widetilde{u}_h(b_1), \widetilde{u}_h(b_0)) \\ &(1-\alpha)\widetilde{u}_h(b_0) + \alpha\min(\widetilde{u}_h(b_2), \widetilde{u}_h(b_0)) \leqslant u_h(m_2) \leqslant (1-\alpha)\widetilde{u}_h(b_0) + \alpha\max(\widetilde{u}_h(b_2), \widetilde{u}_h(b_0)) \\ &(1-\alpha)\widetilde{u}_h(b_0) + \alpha\min(\widetilde{u}_h(b_3), \widetilde{u}_h(b_0)) \leqslant u_h(m_3) \leqslant (1-\alpha)\widetilde{u}_h(b_0) + \alpha\max(\widetilde{u}_h(b_3), \widetilde{u}_h(b_0)) \end{aligned} \tag{25}$$

See Hoteit *et al.* [16, 17] for the solution to this problem. The author shows that the slope limiter eliminates completely spurious oscillations with minimal numerical smearing for $\alpha = 1$.

5. NUMERICAL RESULTS

In this section, we validate and compare the different slope limiters described in the previous section and this on four hydraulic flow problems: the first and the fourth problems are transient problems in a channel during the break of a dam. The second and the third are steady problems, which pass from supercritical flow to subcritical flow through a hydraulic jump. The choice of these four problems for the comparison of the various slope limiters is justified by the following reasons:

- The four problems admit analytical solutions or have experimental data, which makes it possible to compare the simulated solution with the exact solution or the experimental data of the problem.
- The flow in the dam break problems is transient; therefore, the variables vary in time, whereas the flow in the other two problems is steady.
- The solution to these problems contains shocks and discontinuities.

DOI: 10.1002/fld

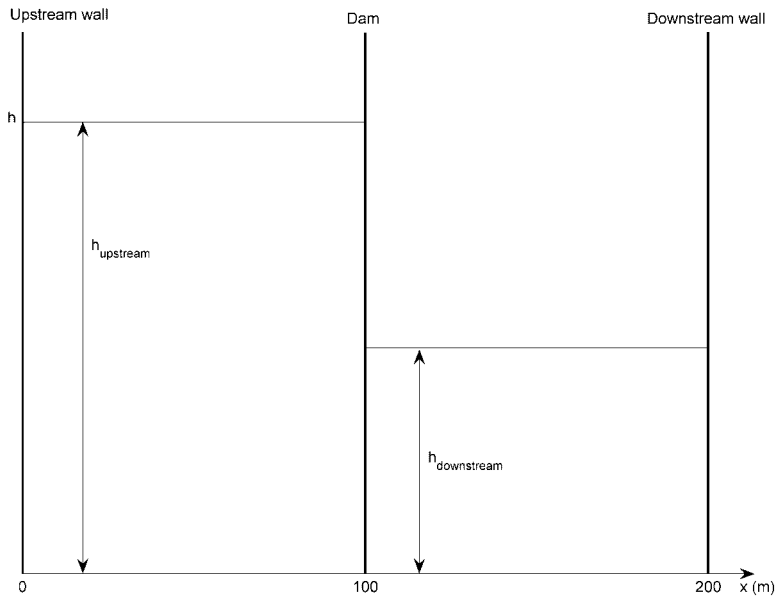

Figure 2. Definition of the dam break problem.

5.1. Test case 1: dam break problem

We consider a horizontal channel of width $B=10\,\text{m}$ and length $L=200\,\text{m}$. The bed of the channel is smooth; therefore, there is no friction effect on the flow. The dam is located at the middle of the channel, and at instant $t=0$, the dam is completely removed and water is slackened in the form of two waves; one moves upstream and the other towards the downstream (Figure 2). The problem domain was triangulated into 672 cells and the computational model was run up to 3 s after the dam break.

In this problem, we are interested in the simulation of the flow during the break of the dam. The initial conditions of the flow are zero flow discharge everywhere in the channel, and a discontinuous water depth at the dam. The water depth at the upstream of the dam is fixed at $h_{\text{upstream}}=10\,\text{m}$, and the water depth at the downstream of the dam varies in order to change the nature of the flow. Since the channel is closed, the flow is reflective at the upstream and the downstream of the channel.

Two cases are considered in order to show the robustness of the slope limiters. In the first case, the flow is subcritical everywhere and therefore the Froude number is lower than 1. In this case, the downstream water depth must be selected so that the depth ratio $h_{\text{downstream}}/h_{\text{upstream}}$ is equal to or greater than 0.5 m ($h_{\text{downstream}}=5\,\text{m}$). Figure 3 shows the water depth results obtained by the different slope limiters.

In the second case, the flow is gradually varied; therefore, it passes from subcritical flow to supercritical flow and inversely. In this case, the downstream water depth must be selected so that the depth ratio $h_{\text{downstream}}/h_{\text{upstream}}$ is lower than 0.5 m ($h_{\text{downstream}}=1\,\text{m}$). Figure 4 shows the water depth results obtained by the different slope limiters.

DOI: 10.1002/fld

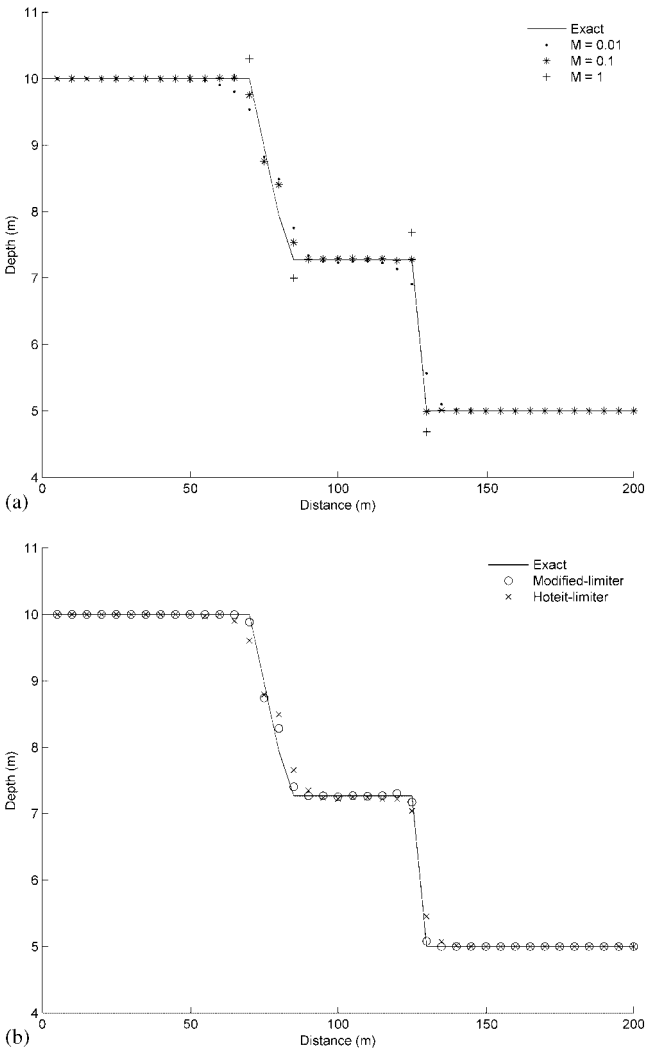

Figure 3. Water depth predicted for the dam break problem (subcritical case): (a) Cockburn and Shu's slope limiter and (b) Hoteit's slope limiter and the modified slope limiter.

Table I shows the relative error in $L2$ norm between the solutions obtained by the different slope limiters and the exact solution for the two cases (subcritical and supercritical). According to Figures 3 and 4, we note that the different slope limiters give similar results in the smooth regions, but notable differences in accuracy are exhibited between these limiters in the regions where the solution is discontinuous. Regarding the results obtained by Cockburn and Shu's slope limiter, it appears that it is not easy to estimate the constant parameter M for the limitation in order to obtain high-order accuracy of the scheme. For a small value of M ($M=0.01$) the slope limiter eliminates oscillations without preserving the high-order accuracy of the scheme. While for a large value of M ($M=1$) the solution is in good agreement in the smooth regions, oscillations appear in the

DOI: 10.1002/fld

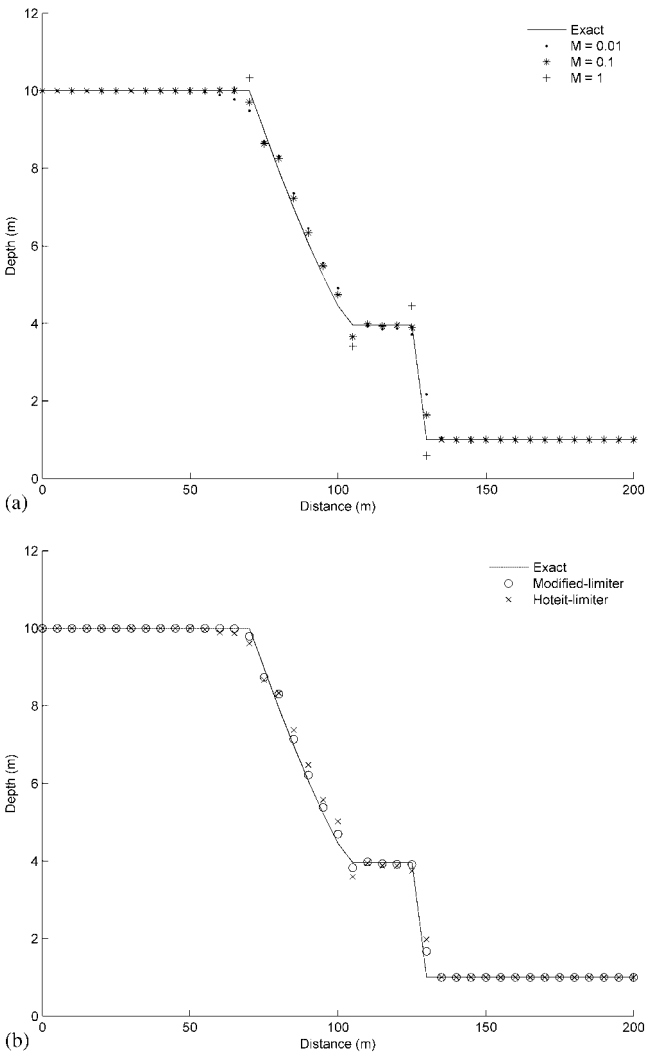

Figure 4. Water depth predicted for the dam break problem (supercritical case): (a) Cockburn and Shu's slope limiter and (b) Hoteit's slope limiter and the modified slope limiter.

discontinuity regions. For $M=0.1$, the slope limiter gives better results. On the other hand, the modified slope limiter performs almost as well. It eliminates the oscillations near discontinuities and preserves the high-order accuracy of the scheme. Moreover, it avoids the difficulty of choosing a constant parameter for limitation. The slope limiter of Hoteit *et al.* gives satisfactory results.

5.2. Test case 2: oblique hydraulic jump problem

The oblique hydraulic jump is induced by means of an interaction between a supercritical flow and a converging wall deflected through an angle $\alpha=8.95°$. The shock wave is formed with

DOI: 10.1002/fld

Table I. Test case 1: $L2$ relative errors of water depth.

	$L2$ error in %	
Slope limiter	Subcritical case	Supercritical case
Cockburn's limiter ($M=0.01$)	2.29	3.81
Cockburn's limiter ($M=0.1$)	1.26	2.41
Cockburn's limiter ($M=1$)	1.68	2.66
Hoteit's limiter	1.93	3.56
Modified limiter	0.94	2.11

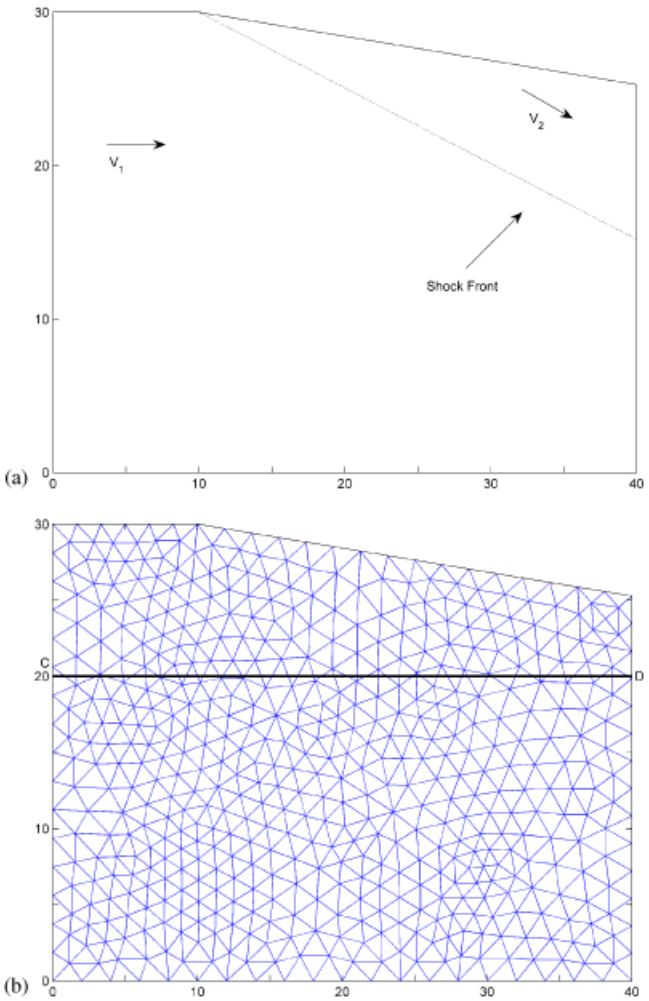

Figure 5. (a) Definition of problem domain for oblique hydraulic jump and (b) the unstructured mesh for oblique hydraulic jump.

DOI: 10.1002/fld

Table II. Test case 2: $L2$ relative errors of water depth and velocity.

	$L2$ error in %	
Slope limiter	Water depth	Velocity
Cockburn's limiter ($M=0.01$)	4.15	0.61
Cockburn's limiter ($M=0.1$)	2.12	0.26
Cockburn's limiter ($M=1$)	2.42	0.39
Hoteit's limiter	3.20	0.42
Modified limiter	1.69	0.19

an angle β. The definition of the problem domain and a schematic diagram of the induced shock front appear in Figure 5(a). The computational domain was triangulated into 1200 cells (Figure 5(b)).

The initial and inflow conditions are the height $h_0=1\,\text{m}$, velocity $u_0=8.57\,\text{m/s}$ and $v_0=0\,\text{m/s}$ (corresponding to a Froude number of 2.74). Fixed boundary conditions are applied at the upstream boundary. Transmissive boundary conditions are imposed at the downstream boundary and slip no-pass boundary conditions at the channel walls. The resulting steady-state flow should be purely supercritical and divided into two regions by an oblique hydraulic jump at an angle of $\beta=30^\circ$ to the upstream flow. Downstream of this jump, the exact solution is given by $h=1.5\,\text{m}$, $|V|=7.9556\,\text{m/s}$ [20].

The quantitative comparison of relative errors in $L2$ norm between the computed results and the analytical solution is shown in Table II. The comparisons of water surface profile and velocity plot along the longitudinal section line ('CD' shown in Figure 5(b)) are represented in Figures 6 and 7, respectively. In the same manner as for the dam break problem, the results indicate that Cockburn and Shu's slope limiter requires a good estimation of the constant parameter M in order to obtain high-order accuracy. On the other hand, the results obtained by the modified slope limiter are slightly better than the others. Moreover, the modified slope limiter avoids the difficulty of choosing any constant parameter.

5.3. Test case 3: flow in a rectangular channel with concave bed

In this section, we consider a hydraulic problem of a flow in a rectangular prismatic channel where the bed has a non-regular geometrical form. The bed of the channel is concave; it has the shape of a bump as indicated in Figure 8.

The length of the channel is 1 km and its width is 1 m. In this example, there are no friction effects. The bump of the bed starts at $x=125\,\text{m}$ and finishes at $x=875\,\text{m}$. The mathematical expression of the bed is given by

$$z(x)=4.75\sin^2\left(\frac{x-125}{750}\pi\right) \tag{26}$$

where z represents the level of the bed compared with a fixed constant altitude, and x is the longitudinal distance. In this example, the flow is subcritical at the upstream, reaches its critical mode at the top of the bump, passes to supercritical mode and finishes in subcritical mode through a hydraulic jump just before the end of the bump.

DOI: 10.1002/fld

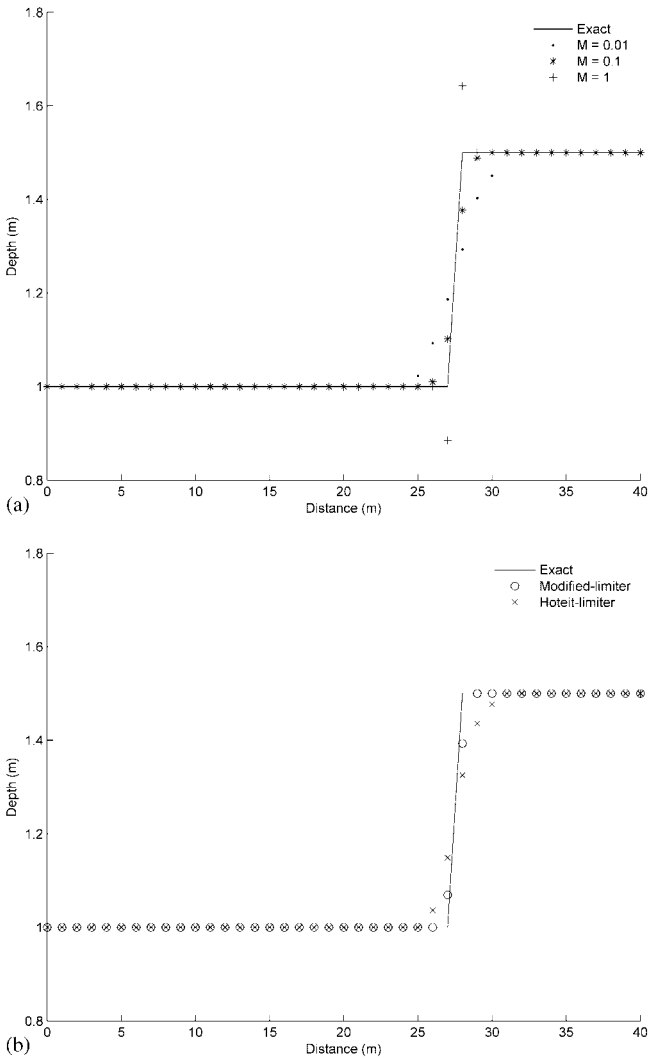

Figure 6. Comparison of the water depth profiles along the longitudinal section line ('CD' shown in Figure 5): (a) Cockburn and Shu's slope limiter and (b) Hoteit's slope limiter and the modified slope limiter.

For the boundary conditions, we imposed a flow discharge $Q = 20\,\mathrm{m}^3/\mathrm{s}$ at the upstream of the channel and a water depth $h = 7\,\mathrm{m}$ at the downstream of the channel. The physical domain is discretized into 3422 triangular cells. The calculated steady-state water surface profiles along the channel centerline are compared with the analytical solution to the problem [21] in Figure 9. In Table III, the relative errors in $L2$ norm of the different slope limiters are compared.

The different slope limiters give similar results in the regions where the solution is smooth but a notable difference in accuracy is exhibited between these limiters in the discontinuity regions.

DOI: 10.1002/fld

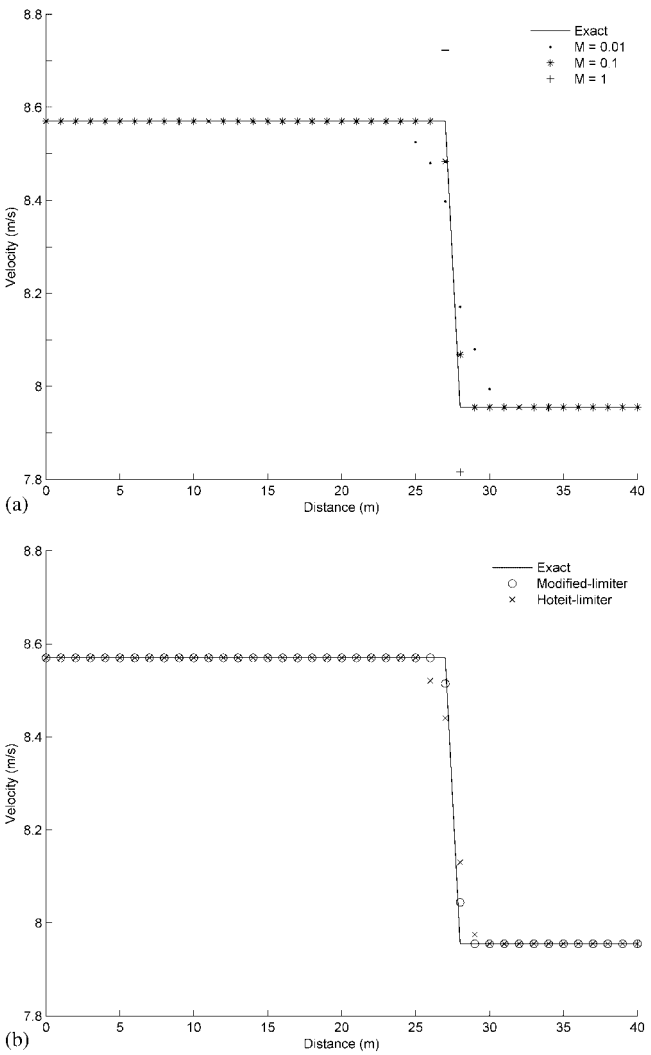

Figure 7. Comparison of the velocity profiles along the longitudinal section line ('CD' shown in Figure 5): (a) Cockburn and Shu's slope limiter and (b) Hoteit's slope limiter and the modified slope limiter.

For Cockburn and Shu's slope limiter, the constant parameter M is difficult to choose in order to obtain good results. In this example, we can see that Cockburn and Shu's slope limiter does not give good results for $M=0.1$ as in the above examples. The high order of the scheme is not preserved in the discontinuity regions. It is also quite the same case for the slope limiter of Hoteit *et al.* For $M=1$, the results obtained by Cockburn and Shu's slope limiter are very close to the analytical solution to the problem. The slope limiter eliminates oscillations near discontinuities and preserves the high-order accuracy of the scheme. By choosing M too large ($M=2$), oscillations appear in the discontinuity regions. The results obtained by the modified slope limiter are also in

DOI: 10.1002/fld

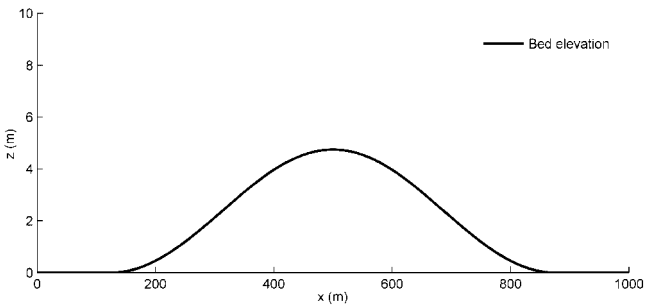

Figure 8. Concave bed of the channel.

good agreement with the analytical solution. The advantage of this modified slope limiter is that it gives high-order accuracy and does not require the estimation of any constant number.

5.4. Test case 4: dam break in a converging–diverging channel

In this example, a dam break wave propagation through a channel constriction is studied. The advancing front is partially reflected by the walls of the contraction producing a smooth front downstream of the channel. Subcritical and supercritical flows are produced along the channel. The geometry of the model is detailed in Figure 10. It consists of a rectangular channel (19.3 m long, 0.5 m wide). The dam is located 6.1 m downstream of the first section of the channel. The first constriction section is situated 7.7 m downstream of the dam. The constriction is 1 m long and 0.1 m wide and forms a 45° angle with the channel walls. The bottom is flat.

Initial conditions are still water steady state with 0.3 m water depth upstream the dam and 0.25 m downstream. Boundary conditions are solid walls except at the outlet that is considered free. Manning coefficient is 0.01. The mesh uses 10 578 triangular cells.

Figure 11 shows the comparison between the experimental data and the numerical results of the water depth time evolution during 10 s at the three gauging points $S1$, $S2$ and $S3$. As shown in Figure 10, $S1$ is situated before the constriction and we will see the arrival of the dam break front and the reflected front produced in the walls of the constriction. $S2$ is at the middle of the constriction and there we can only see the arrival of a smoother front and finally $S3$ is after the constriction. The relative errors in $L2$ norm between the results obtained by the different slope limiters and the experimental data are listed in Table IV.

According to Figure 11, the slope limiter of Cockburn and Shu is not able to deal with strong discontinuities for a small value of M ($M=0.1$) and the high order of the scheme is not preserved. By choosing $M=1$, we find that the results are in good agreement with the experimental data. For large value of M ($M=2$), oscillations appear in the discontinuity regions. However, the modified slope limiter gives the best agreement compared with the experimental data. It is clear that the results obtained by the modified slope limiter are also close to those obtained by Cockburn and Shu's slope limiter for the value of M equal to 1, but as said previously, the advantage of this limiter is that it avoids the difficulty of choosing the constant parameter M. The slope limiter of Hoteit *et al.* eliminates oscillations without preserving the high-order accuracy of the scheme as the modified slope limiter does.

DOI: 10.1002/fld

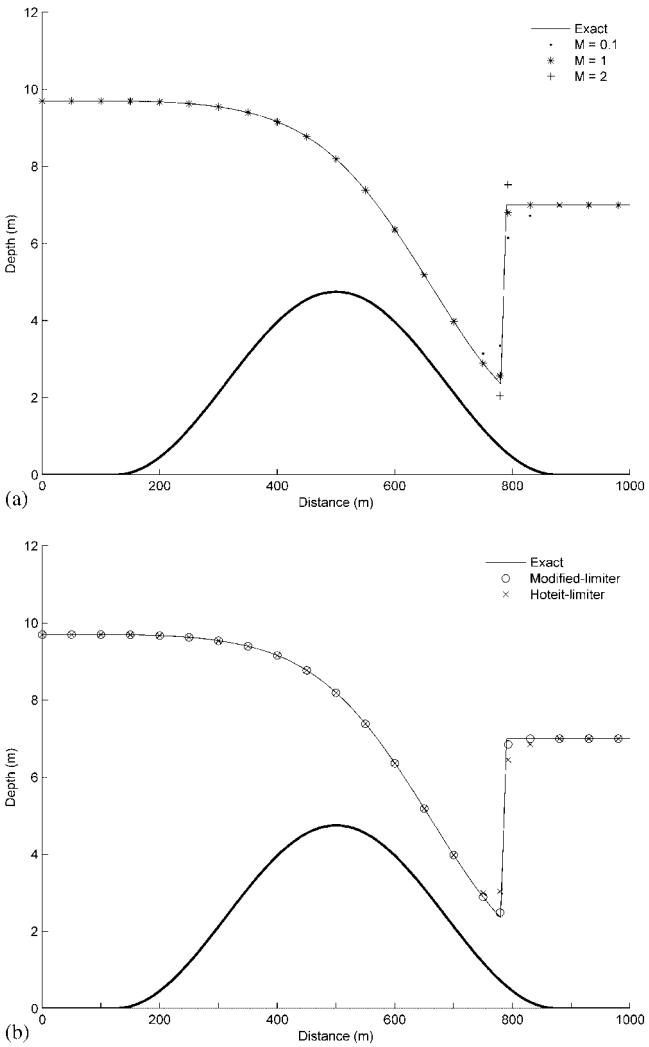

Figure 9. Comparison between the analytical solution and the numerical solution of the water depth: (a) Cockburn and Shu's slope limiter and (b) Hoteit's slope limiter and the modified slope limiter.

Table III. Test case 3: $L2$ relative errors of water depth.

Slope limiter	$L2$ error in %
Cockburn's limiter ($M=0.1$)	3.68
Cockburn's limiter ($M=1$)	0.77
Cockburn's limiter ($M=2$)	1.63
Hoteit's limiter	2.42
Modified limiter	0.54

DOI: 10.1002/fld

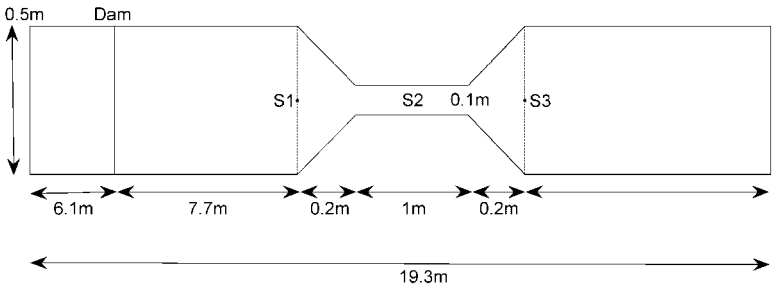

Figure 10. Geometry of the physical model.

Table IV. Test case 4: $L2$ relative errors of water depth at the three gauging points $S1$, $S2$ and $S3$.

	$L2$ error in %		
Slope limiter	$S1$	$S2$	$S3$
Cockburn's limiter ($M=0.1$)	3.26	3.31	1.39
Cockburn's limiter ($M=1$)	0.93	0.88	0.46
Cockburn's limiter ($M=2$)	1.29	1.48	1.48
Hoteit's limiter	2.19	2.45	1.08
Modified limiter	0.65	0.76	0.34

6. CONCLUSION

In this paper, two existing slope limiters for a two-dimensional, high-order RKDG method on unstructured triangular meshes (Cockburn's slope limiter and Hoteit's slope limiter) are described. The disadvantage of these slope limiters is that the limiter condition depends on a constant number. The choice of this number is sometimes not simple to completely eliminate oscillations near discontinuities and preserve the high-order accuracy of the scheme. A simple modification of Cockburn's slope limiter is introduced to avoid the use of this number. Therefore, the limiter condition depends only on the neighboring solution averages. Four hydraulic problems of discontinuous solutions of two-dimensional shallow water are solved by the RKDG method with the different slope limiters quoted above. Verifications of all the numerical results are made by comparison with analytical solutions or experimental data. Based on solving the idealized dam break problem, the oblique hydraulic jump problem, flow in a channel with concave bed and the dam break problem in a converging–diverging channel, it can be concluded that the results of the different slope limiters perform almost well in the regions where the solution is smooth but a remarkable difference in accuracy is exhibited between these limiters in the discontinuity regions. On the other hand, it is not easy to choose the constant number needed in the limitation for Cockburn and Shu's slope limiter in order to obtain good results. We have seen that this limiter and the modified slope limiter perform equally well for such specific value of M. However, if M is chosen too small, Cockburn and Shu's slope limiter eliminates oscillations without preserving the high-order accuracy of the scheme; however, if M is chosen too large, oscillations will appear. In the meantime, the presented modified slope limiter gives almost the best results, avoids all oscillations and preserves the

DOI: 10.1002/fld

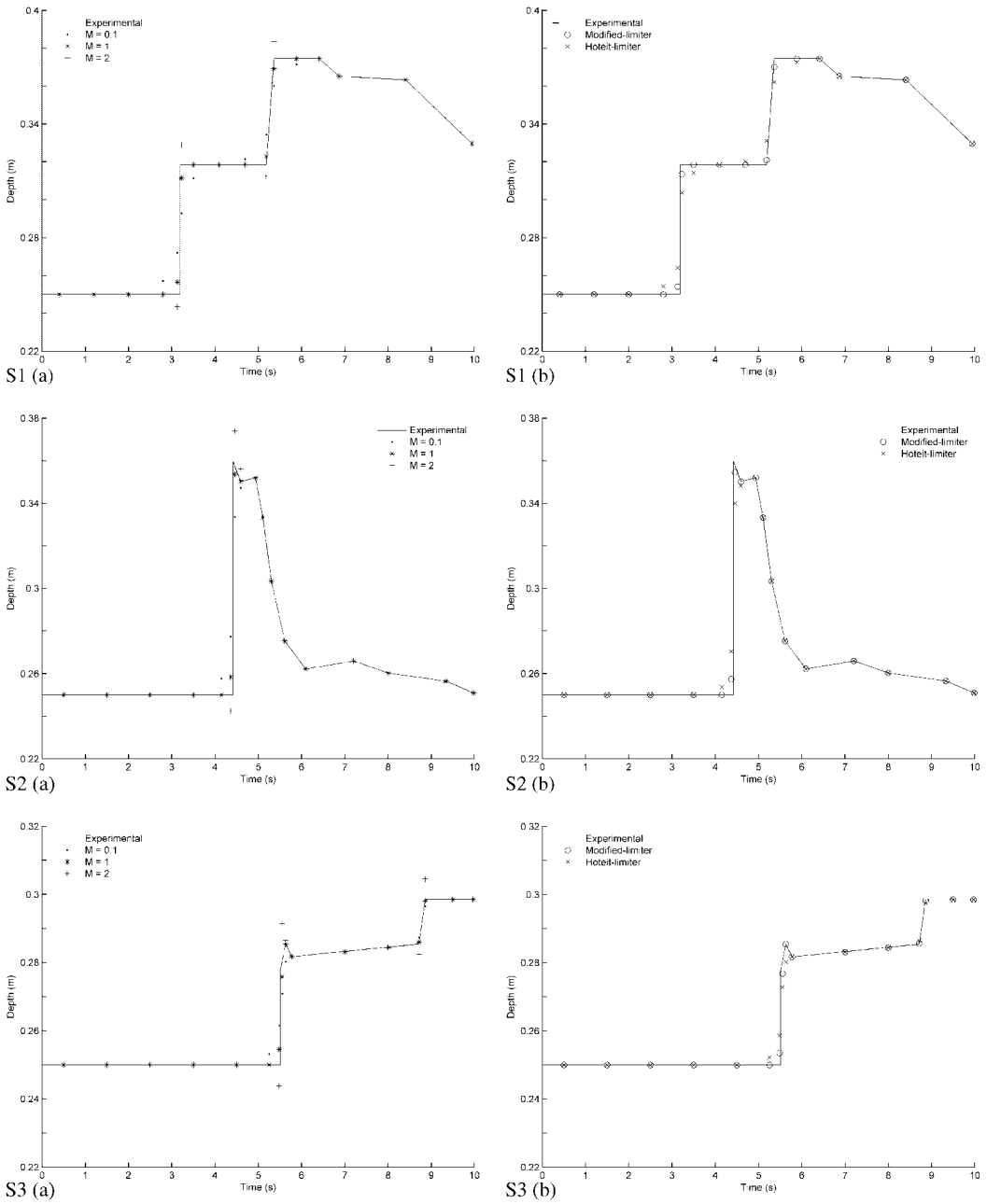

Figure 11. Comparison between the experimental data and the numerical results on the time evolution during 10 s of the water depth at the gauging points *S*1, *S*2 and *S*3: (a) Cockburn and Shu's slope limiter and (b) Hoteit's slope limiter and the modified slope limiter.

DOI: 10.1002/fld

high-order accuracy of the scheme. Moreover, it avoids the difficulty of choosing a specific constant for the limitation, as it is the case with the other slope limiters.

REFERENCES

1. Cockburn B, Hou S, Shu CW. TVB Runge–Kutta local projection discontinuous Galerkin finite element method for conservation laws III: one-dimensional systems. *Journal of Computational Physics* 1989; **84**:90–113.
2. Cockburn B, Shu CW. The Runge–Kutta discontinuous Galerkin method for conservative laws V: multidimensional systems. *Journal of Computational Physics* 1998; **141**:199–224.
3. Kessewani G, Ghostine R, Vazquez J, Ghenaim A, Mosé R. Application of a second-order Runge–Kutta discontinuous Galerkin scheme for the shallow water equations with source terms. *International Journal for Numerical Methods in Fluids* 2008; **56**:805–821.
4. Schwanenberg D, Harms M. Discontinuous Galerkin finite-element method for transcritical two-dimensional shallow water flows. *Journal of Hydraulic Engineering* 2004; **130**(5):412–421.
5. Goodman J, LeVeque R. On the accuracy of stable schemes for 2D scalar conservation laws. *Mathematics of Computation* 1985; **45**:15–21.
6. Harten A. High resolution schemes for hyperbolic conservation laws. *Journal of Computational Physics* 1983; **49**:357–393.
7. Harten A, Hyman J, Lax P. On finite-difference approximations and entropy conditions for shocks. *Communications on Pure and Applied Mathematics* 1976; **29**:297–322.
8. Godunov S. Finite difference methods for numerical computation of discontinuous solutions of the equations of fluid dynamics. *Mathematics of the USSR—Sbornik* 1959; **47**:271–306.
9. Van Leer B. Towards the ultimate conservative scheme: II. *Journal of Computational Physics* 1974; **14**:361–376.
10. Van Leer B. Towards the ultimate conservative scheme: IV. A new approach to numerical convection. *Journal of Computational Physics* 1977; **23**:276–299.
11. Van Leer B. Towards the ultimate conservative scheme: V. A second order Godunov's method. *Journal of Computational Physics* 1979; **32**:101–136.
12. Hirsh C. *Numerical Computation of Internal and External Flows*. Wiley Interscience: New York, 1990.
13. Toro E. *Riemann solvers and Numerical Methods for Fluid Dynamics*. Springer: Berlin, 1997.
14. Cockburn B, Shu CW. TVB Runge–Kutta local projection discontinuous Galerkin finite element method for conservation laws II: general framework. *Mathematics of Computation* 1989; **52**:411–435.
15. Shu CW. TVB uniformly high order schemes for conservation laws. *Mathematics of Computation* 1987; **49**: 105–121.
16. Hoteit H. Simulation d'écoulements et de transports de polluants en milieu poreux: Application à la modélisation de la sureté des dépots de déchets radioactifs. *Thesis*, Rennes University, France, 2002.
17. Hoteit H, Ackerer Ph, Mosé R, Erhel J, Philippe B. New two-dimensional slope limiters for discontinuous Galerkin methods on arbitrary meshes. *International Journal for Numerical Methods in Engineering* 2004; **61**(14):2566–2593.
18. Chavent G, Jaffré J. *Mathematical Models and Finite Elements for Reservoir Simulation*. Studies in Mathematics and its Applications. Elsevier: Amsterdam, 1986.
19. Schwanenberg D. Die Runge–Kutta Discontinuous Galerkin Methode zur Losung konvektionsdominierter tiefengemittelter Flachwasserprobleme. *Thesis*, Aachen University, Germany, 2003.
20. Alcrudo F, Garcia-Navarro P. A high-resolution Godunov-type scheme in finite volumes for the 2D shallow-water equations. *International Journal for Numerical Methods in Fluids* 1993; **16**:489–505.
21. Garcia-Navarro P, Alcrudo F, Saviron JM. 1-D open channel flow simulation using TVD-MacCormack scheme. *Journal of Hydraulic Engineering* 1992; **118**:1359–1372.

DOI: 10.1002/fld